RESEARCH ARTICLE

Metallothioneins and Zinc Dysregulation Contribute to Neurodevelopmental Damage in a Model of Perinatal Viral Infection

Brent L. Williams[1,2]; Kavitha Yaddanapudi[1]; Cassandra M. Kirk[1]; Arya Soman[1]; Mady Hornig[1]; W. Ian Lipkin[1]

[1] Greene Infectious Disease Laboratory, Mailman School of Public Health, Columbia University, New York, NY.
[2] Department of Microbiology and Molecular Genetics, University of California, Irvine.

Corresponding author:
Dr W. Ian Lipkin, Jerome L. and Dawn Greene Infectious Disease Laboratory, Mailman School of Public Health, Columbia University, 722 West 168th Street, Rm 1801, New York, NY 10032 (E-mail: *wil2001@columbia.edu*)

Neonatal Borna disease (NBD) virus infection in the Lewis rat results in life-long viral persistence and causes behavioral and neurodevelopmental abnormalities. A hallmark of the disorder is progressive loss of cerebellar Purkinje and dentate gyrus granule cells. Findings of increased brain metallothionein-I and -II (MT-I/-II) mRNA expression in cDNA microarray experiments led us to investigate MT isoforms and their relationship to brain zinc metabolism, cellular toxicity, and neurodevelopmental abnormalities in this model. Real-time PCR confirmed marked induction of MT-I/-II mRNA expression in the brains of NBD rats (40.5-fold increase in cerebellum, $p<0.0001$; 6.8-fold increase in hippocampus, $p=0.003$; and 9.5-fold increase in striatum, $p=0.0012$), whereas a trend toward decreased MT-III mRNA was found in hippocampus (1.25-fold decrease, $p=0.0841$). Double label immunofluorescence revealed prominent MT-I/-II expression in astrocytes throughout the brain; MT-III protein was decreased in granule cell neurons and increased in astrocytes, with differential subcellular distribution from cytoplasmic to nuclear compartments in NBD rat hippocampus. Modified Timm staining of hippocampus revealed reduced zinc in mossy fiber projections to the hilus and CA3, accumulation of zinc in glial cells and degenerating granule cell somata, and robust mossy fiber sprouting into the inner molecular layer of the dentate gyrus. Zinc Transporter 3 (ZnT-3) mRNA expression was decreased in hippocampus (2.3-fold decrease, $p=0.0065$); staining for its correlate protein was reduced in hippocampal mossy fibers. Furthermore, 2 molecules implicated in axonal pathfinding and mossy fiber sprouting, the extracellular matrix glycoprotein, tenascin-R (TN-R), and the hyaluronan receptor CD44, were increased in NBD hippocampal neuropil. Abnormal zinc metabolism and mechanisms of neuroplasticity may contribute to the pathogenesis of disease in this model, raising more general implications for neurodevelopmental damage following viral infections in early life.

Brain Pathol 2006;16:1-14.

INTRODUCTION

Borna disease virus (BDV) is a neurotropic RNA virus that infects a wide variety of warm-blooded animals. Lewis rats experimentally infected as adults have meningoencephalitis and a progressive movement disorder; infected neonates do not mount a cellular immune response to infection, yet have microglial activation, proinflammatory cytokine gene expression, cerebellar and hippocampal dysgenesis, and disturbances of learning, mood and behavior (neonatal Borna disease, NBD) (6). Although BDV is noncytolytic, neuronal apoptosis is observed in cerebellum and hippocampus in NBD (25, 62). However, the cellular and molecular mechanisms responsible for loss of specific neuronal subsets are unknown. Damage is proposed to result from virus-mediated obstruction of cellular proliferation, differentiation, or survival pathways. NBD is associated with altered brain levels of transcripts encoding cytokines (IL-1β, IL-6, TNF-α, and TGF-β1); neurotrophic factors (brain-derived neurotrophic factor [BDNF], nerve growth factor [NGF], and neurotrophin-3 [NT-3]); neurotransmitters and receptors (serotonin, dopamine); and apoptosis-related products (Fas, caspase-1, and Bcl-x) (6, 25). Decreased levels of 2 presynaptic proteins involved in synaptic plasticity, synaptophysin and GAP-43, are observed in regions of neuronal loss (22). Functional disturbances of infected astrocytes may also contribute to pathogenesis in NBD. Astrocytes are intimately associated with neuronal synapses and regulate glutamate uptake/release and secretion of soluble factors that promote neurogenesis, neuron survival, and neurite extension (1, 41, 54). Persistent BDV infection of primary feline cortical astrocytes results in inhibition of glutamate uptake (3).

The role of zinc in normal brain maturation and in disturbances of neurodevelopmental processes has only begun to be examined. Although zinc homeostasis may play a regulatory role during neurotransmission, it has been suggested that zinc may also contribute to neuronal injury in pathological contexts. High levels of zinc are toxic to both neuronal and non-neuronal cells in vitro (13, 66) and neuronal zinc accumulation correlates with neurodegeneration in models of brain injury (20, 33, 55, 56). Nonetheless, zinc is indispensable for normal brain development and is required for the function of over 200 enzymes and proteins (59). Zinc is abundant in the normal brain and gradually increases during early postnatal development (neonatal growth spurt), with high concentrations in the cerebellum of neonates and in the hippocampus of adult rats (49). The majority of brain zinc is associated with metalloprotein complexes. The remaining zinc (approximately 10%) is localized at synaptic vesicles in a subset of glutamatergic neurons (19). Particularly high concentrations of zinc are found in hippocampal granule cell mossy fibers, where zinc is released along with glutamate during synaptic transmission and may serve as an endogenous neuromodulator of NMDA, AMPA, and GABA receptors and the glial glutamate transporter, EAAT1 (13, 60). Homeostatic controls over zinc

Gene (Accession #)	Primer Pairs (5′–3′) [Reaction Concentration] and probe	Amplicon (bp)
MT-I/ -II (J00750)	For: AGGGCTGTGTCTGCAAAGGT [100nm] Rev: CAAGACTCTGAGTTGGTCCGG [100nm] FAM-ACGTGCTGTGCCTGAAGTGACGAAC-TAMRA	110
MT-III (BC058453)	For: TACAGTCTCTCGCGGCTGCT [100nm] Rev: GCAGCTCTTCTTGCAGTTCGT [100nm] FAM-CCTGTCCTACTGGTGGTTCCTGCACCT-TAMRA	130
ZnT-3 (AY538655)	For: AAGCCCCAGTACAAGGTGGC [300nm] Rev: ACCTTCCATGAGGACGAGGA [300nm] FAM-CAGCACCTTCCTCTTCTCTATCTGCGCC-TAMRA	110
ZnT-1 (U17133)	For: GGACCAGGCAGAGCCAGAG [300nm] Rev: GGACGTGCAGAAACACTCCTC [300nm] FAM-AATGGGAATCTCATCCAGGAGTCAGACAGTC-TAMRA	145
PBGD (X06827)	For: ATTCGGGGAAACCTCAACACC [300nm] Rev: CTGACCCACAGCATACATGCAT [300nm] FAM-GCAAGATCTGGCCCACCCGGTT-TAMRA	157

Table 1. *Real-time PCR: rat gene-specific, primer and probe combinations.* Accession numbers are given for sequence used to design primer and probe sets using Primer Express software. The final concentration of primers used in real-time PCR reactions and amplicon size are indicated.

bioavailability, vesicular storage/sequestration, and cellular influx and extrusion are mediated in large part by zinc-sequestering proteins (metallothioneins and albumin), amino acids (histidine and cysteine) and a family of zinc transporters (ZnT1-ZnT4) (17, 57). Zinc is a potent physiological inducer of metallothionein (MT) expression through the zinc-dependent transcription factor, MTF-1, and metal response elements in the promoter of MT genes (23). Conversely, MT is also intimately involved in the regulation of zinc homeostasis and bioavailability (29).

Here, we describe evidence that abnormalities in zinc regulatory systems may contribute to the pathology of NBD. Our findings are consistent with other forms of zinc-associated neurodegeneration and may have general implications for understanding how infections in early life cause neurodevelopmental damage.

MATERIALS AND METHODS

Animals. Lewis rat dams were obtained from Charles River Laboratories (Wilmington, Mass). Within 12 hours of birth, Lewis rat pups were inoculated into the right cerebral hemisphere with 50 µl of 5×10^3 tissue culture infectious units of BDV strain He/80-1 (NBD) or phosphate buffered saline (control). Rats were sacrificed at 4 weeks of age for nucleic acid, protein and anatomic analyses.

RNA extraction. At 4 weeks post inoculation NBD (n = 7) and control (n = 5) rats were terminally anesthetized with CO_2. Brain regions (cerebellum, hippocampus, and striatum) were immediately dissected, snap frozen in TRIzol (Invitrogen, Carlsbad, Calif), and stored at -80°C. Total RNA was extracted from cerebellum, hippocampus, and striatum of individual animals using acid phenol extraction.

Microarray analysis. Equal amounts of total RNA extracted from either cerebellum or hippocampus of individual animals were pooled to create a single control RNA sample (n = 5 control rats) and an NBD RNA pool (n = 7 NBD rats) for use in microarray assays. Indirect labeling and cDNA synthesis were performed using 3DNA Array 350 Expression Array Detection Kit for Microarrays (Genisphere, Hatfield, Pa). Five µg of RNA were reverse transcribed using random primers tagged with either Cy3 (BDV pool) or Cy5 (Control pool) 3DNA capture sequences. After combining Cy3 and Cy5 capture sequence-labeled products, cDNA was ethanol precipitated, resuspended in water and hybridized to a rat 8K oligonucleotide array (Center for Applied Genomics, Public Health Research Institute, Newark, NJ) using the 3DNA Array 350 kit. Briefly, Genisphere 3DNA tagged cDNA was incubated at 80°C for 10 minutes with a SDS-based hybridization buffer containing denatured human Cot-1 DNA (1 µg/40 µl, Invitrogen/Gibco LTI, Gaithersburg, Md) before applying to the prewarmed microarray in a humidified hybridization chamber. After hybridization at 53°C for 18 hours, slides were washed for 15 minutes each in 2 × SSC/0.2% SDS at 42°C, 2 × SSC at room temperature, 0.2 × SSC at room temperature, and then dried by centrifugation. The hybridized cDNA was fluorescence-labeled during an additional hybridization with the Cy3-3DNA and Cy5-3DNA capture reagents in SDS-hybridization buffer for 3 hours at 62°C, followed by sequential washes for 15 minutes each in 2 × SSC/0.2%SDS at 65°C, and 2 × SSC and 0.2 × SSC at room temperature. Fluorescence-labeled slides were dried by centrifugation and scanned with a GenePix 4000B scanner (Axon Instruments, Inc., Union City, Calif) at 5-µm resolution; variable gains were used on the photomultiplier tube to acquire high intensity scans without oversaturation. For each spot, background-subtracted signal intensity, acquired using GenePix Pro 4.1 software, was normalized for both Cy3 and Cy5 expression by scaling individual spot intensities in each channel to the total intensity of all spots on the array. Microarray experiments using cerebellar and hippocampal RNA sets were performed in triplicate. Data were paired for each array, and analyzed using the Cyber T web interface (*http://visitor.ics.uci.edu/genex/cybert/*). Differences in gene hybridization signal that met the following criteria were considered to be significant: fold-change greater than 2.0 or less than -2.0, and $p<0.05$ (paired t-test).

Quantitative real-time PCR. Intron/exon spanning, gene-specific PCR primers and fluorophore-labeled oligonucleotide probes specific for rat Metallothionein-I and -II (MT-I/-II), Metallothionein-III (MT-III), Zinc Transporter 3 (ZnT-3), Zinc Transporter 1 (ZnT-1), and Porphobilinogen Deaminase (PBGD) as housekeeping gene control were designed for real-time PCR using Primer Express 1.0 software (Applied Biosystems (ABI), Foster City, Calif) (Table 1). The probes were labeled with a 5′-end fluorescent reporter dye, 6-carboxyfluorescein (FAM), and a 3′-end quencher dye, 6-carboxy-tetramethyl-rhodamine (TAMRA). PCR standards for determining gene copy number of the target transcript were created by cloning the region of the gene

to be analyzed into the pGEM-T easy vector (Promega Corporation, Madison, Wis). Linearized plasmid was quantitated by UV spectroscopy and 10-fold serial dilutions were created in distilled water containing yeast tRNA (1 ng/µl) ranging from 5×10^6 to 5×10^1 copies for MT-I/-II, 5×10^5 to 5×10^1 copies for MT-III, 5×10^5 to 5×10^0 copies for ZnT-3, and 5×10^5 to 5×10^1 for ZnT-1. RNA from hippocampus, cerebellum or striatum of individual animals was used for real time PCR assays. cDNA was synthesized using Taqman reverse transcription reagents (ABI) from 2-µg unpooled RNA per 100-µl reaction from either the cerebellum, hippocampus, or striatum of each of 7 NBD rats and 5 control rats; each sample was assayed in triplicate. For MT-I/-II real-time PCR, cDNA was diluted 1:100 due to the high copy number obtained in brain tissue. For all other genes cDNA was used undiluted. Each 25-µl amplification reaction contained 10 µl template cDNA, 12.5 µl Universal Master Mix (ABI), 200-nM probe, and the primer concentrations given in Table 1. The thermal cycling profile using a Model 7700 Sequence Detector System (ABI) consisted of: Stage 1, one cycle at 50°C for 2 minutes; Stage 2, one cycle at 95°C for 10 minutes; Stage 3, 45 cycles at 95°C for 15 seconds and 60°C for one minute. To control for mRNA integrity and PCR efficiency, a porphobilinogen deaminase (PBGD) fragment was amplified in triplicate reactions by real-time PCR on the same plate as the gene of interest. The mean concentration of PBGD in each sample, based on triplicate values, was used to control for integrity of input mRNA and to normalize values of target gene expression to those of the housekeeping gene expression. The final results are expressed as the mean number of copies per 200 ng total RNA for MT-III, ZnT-3, and ZnT-1 and mean number of copies per 1:100 dilution of 200 ng total RNA for MT-I/-II, relative to values obtained for PBGD mRNA. A negative control lacking cDNA template was included with each assay to confirm specificity. For verification of single amplification products, PCR reactions were examined by 1.5% agarose gel electrophoresis.

Metallothionein western immunoblot. Hippocampus, striatum, and cerebellum were dissected from 4-week-old NBD and control rats and homogenized in PBS containing protease inhibitors (Complete Mini, EDTA-free tablets, Roche Molecular Biochemicals, Indianapolis, Ind). Homogenates were centrifuged at 12 000 rpm for 15 minutes at 4°C. Supernatants were collected and protein concentrations estimated by Bradford assay (Bio-Rad, Hercules, Calif). Proteins from regional brain homogenate (20 µg) in sample buffer (10 mM Tris-HCl, pH 7.5; 10 mM EDTA, 20% v/v glycerol; 1% w/v SDS; 0.005% w/v bromphenol blue; 100 mM dithiothreitol) were boiled for 5 minutes and size fractionated by 18% SDS-PAGE. Gels and 0.2-µm nitrocellulose membranes (Pierce Biotechnology, Inc., Rockford, Ill) were briefly equilibrated in transfer buffer (25 mM Tris-HCl, pH 8.3; 192 mM glycine; 20% methanol; 2 mM $CaCl_2$) before transferring proteins to membranes using a semi-dry blotting apparatus (Owl Separation Systems, Portsmouth, NH). Following transfer, membranes were incubated in 2.5% glutaraldehyde in water for one hour at room temperature, washed 2×10 minutes in PBS, followed by an additional 10-minute wash with 50 mM monoethanolamine in PBS. Membranes were blocked in 2% nonfat milk powder in TTBS (20 mM Tris-HCl, pH 7.6; 137 mM NaCl; 0.1% Tween 20) overnight at room temperature and incubated with mouse anti-horse MT-I/-II mAb (1:500, clone E9, DAKO Cytomation, Carpinteria, Calif) in TTBS containing 1% nonfat dry milk for 2 hours at room temperature. Membranes were washed 3×10 minutes with TTBS prior to incubation with horseradish peroxidase-conjugated goat anti-mouse IgG (Bio-Rad, 1:1000) in TTBS with 1% nonfat dry milk for one hour at room temperature. Membranes were washed again with TTBS, developed using ECL western blot detection system (Amersham Biosciences, Arlington Heights, Ill) and scanned for chemiluminescence using a Storm 840 Imager (Amersham Biosciences/Molecular Dynamics). Bands at 14 kDa were interpreted as representing MT-I; bands at 11 kDa were interpreted as representing MT-II.

Immunofluorescence/immunohistochemistry. Under CO_2 anesthesia, NBD (n = 4) and control (n = 4) rats were perfused via left ventricular puncture with PBS (1 ml/g body weight), followed by buffered 4% paraformaldehyde (1 ml/g body weight). Brains were post-fixed in 4% paraformaldehyde overnight at 4°C, and cryoprotected with graded sucrose solutions. Cryostat sections (14 µm) were collected onto glass slides (Super Frost Plus, Fisher Scientific, Pittsburgh, Pa). For immunofluorescence microscopy, sections were rinsed for 5 minutes in PBS, followed by treatment with 0.1% TritonX-100 in PBS for one hour at room temperature. Sections were again washed with PBS for 5 minutes and then blocked with 10% goat serum in PBS for one hour at 37°C. Sections were incubated with primary antibodies (mouse anti-horse MT-I/-II mAb [1:50, DAKO Cytomation], rabbit anti-rat MT-III Ab [1:250, kind gift of Juan Hidalgo (7)], rabbit anti-GFAP Ab [1:100, DAKO], mouse anti-GFAP mAb cocktail [1:30, BD Pharmingen, San Diego, Calif], rabbit anti-Iba1 Ab [2 µg/ml, Wako Pure Chemical Industries, Ltd., Richmond, Va], rabbit anti-synaptophysin Ab [1:50, Santa Cruz Biotechnology, Santa Cruz, Calif], anti-rat CD44H Ab [1:50, BD Pharmingen], anti-rat tenascin R mAb [1:10, R&D Systems, Minneapolis, Minn]) in blocking solution at 4°C overnight. After 3 washes in PBS, sections were incubated with Cy3-conjugated anti-mouse IgG or Cy3-conjugated anti-rabbit IgG (1:200, Jackson Immunoresearch Laboratories, Inc., West Grove, Pa) and/or Cy2-conjugated anti-rabbit IgG (1:200, Jackson Immunoresearch) or Cy2-conjugated anti-mouse IgG in PBS for one hour at room temperature. Sections were washed 3× in PBS, dehydrated through graded ethanol solutions, placed in Americlear and mounted with Permount (Fisher Scientific) for microscopic analysis. ZnT-3 and MT-III immunohistochemistry were carried out according to Wenzel et al (63) with minor modifications. Sections were rinsed sequentially in PB, pH 7.4 (0.1 M sodium phosphate monobasic dihydrate, 0.1 M sodium phosphate dibasic heptahydrate) and 0.1 M Tris-HCl, pH 7.4 (TB) for 5 minutes each, incubated at room temperature in TB containing 1% H_2O_2 for 2 hours, and then blocked in 3% BSA/3% goat serum/0.25% DMSO in TBS (0.05 M TB, pH 7.4, 0.15 M NaCl) for one hour at room temperature. After rinsing for 30 minutes in TBS, sections were incubated for 20 hours at 4°C in affinity purified rabbit anti-mouse ZnT-3 antiserum [1:100, kind gift of Richard Palmiter (43)] or rabbit anti-rat MT-III an-

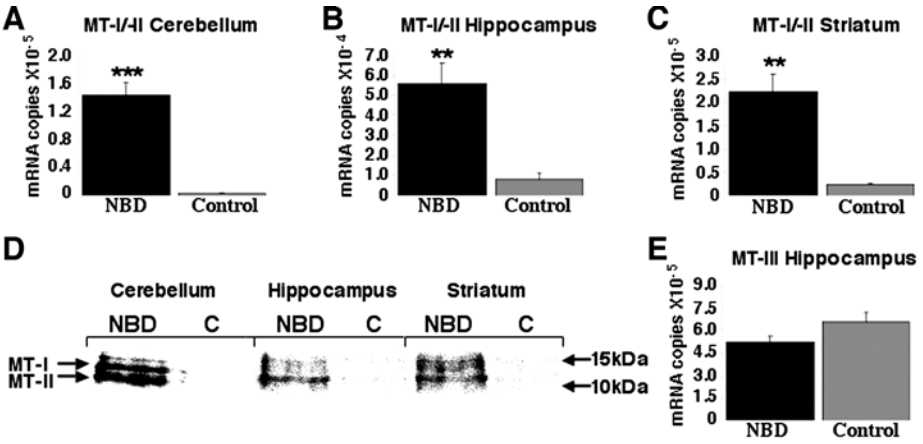

Figure 1. *MT-I/-II and MT-III mRNA and MT-I/II protein expression in 4 week NBD and control rat brains.* **A-C.** Real time PCR for MT-I/-II; (**D**) western immunoblot; (**E**) real time PCR for MT-III. **A**. MT-I/-II mRNA levels in cerebellum; NBD (n = 7), control (n = 5); 40.5-fold increase in NBD: ANOVA, p<0.0001. **B.** MT-I/-II transcript levels from hippocampal RNA; NBD (n = 7), control (n = 5); 6.8-fold increase in NBD: ANOVA, p = 0.003. **C.** MT-I/-II transcript levels from striatum mRNA; NBD (n = 7), controls (n = 5); 9.5-fold increase in NBD: ANOVA, p = 0.0012. **D.** MT-I and MT-II proteins in cerebellum, hippocampus, and striatum. Lanes represent pooled homogenates from 4 NBD and 4 control (**C**) rats. Results were similar with homogenates from individual animals. NBD rats have higher signal for MT-I and MT-II. Signal for MT-II is higher than MT-I in NBD hippocampus. **E.** MT-III mRNA levels in hippocampus; NBD (n = 7), control (n = 5); 1.25-fold decrease in NBD: ANOVA, p = 0.0841. Double asterisk indicates p<0.01; triple asterisk indicates p<0.0001 relative to control rats (ANOVA).

tiserum [1:250] in TBS with 2% BSA/1% goat serum/0.25% DMSO. After rinsing in TBS for 2 hours, sections were incubated with biotinylated goat anti-rabbit IgG (1:200, Vector Laboratories, Burlingame, Calif) for 24 hours at 4°C. Sections were then rinsed with TBS for 2 hours, incubated with ABC reagent (Elite ABC kit, Vector Laboratories) diluted in TBS containing 2% BSA/1% goat serum/0.25% DMSO for 24 hours at 4°C, rinsed in TB, pH 7.6, and incubated with 3,3′-diaminobenzidine solution (DAB peroxidase substrate kit, Vector Laboratories) for 15 minutes at room temperature. Slides were rinsed in distilled water, dehydrated through graded ethanol solutions, placed in Americlear and coverslipped with Permount (Fisher Scientific).

Modified Timm stain. Under CO_2 anesthesia, NBD (n = 4) and control (n = 4) rats were perfused via left ventricular puncture with PBS, followed by 0.1% sodium sulfide solution (13 mM $Na_2S \cdot 9H_2O$, 86 mM $NaH_2PO_4 \cdot H_2O$ in 1 L distilled water), and then with buffered 4% paraformaldehyde (1 ml/g body weight for each perfusate). Brains were post-fixed in 4% paraformaldehyde overnight at 4°C, and cryoprotected with graded sucrose solutions. Cryostat sections (14 µm) were collected onto glass slides (Super Frost Plus) and immediately processed for Timm staining according to Sloviter (52). Timm developer was prepared freshly before each use. Slides were covered in developer in a dark room for 30, 45, 60, 75, and 90 minutes to compare development times. The reaction was stopped in the dark by immersing slides in water. Slides were counterstained with cresyl violet for 5 minutes, rinsed 2 × 5 minutes in water, dehydrated through graded ethanol solutions, placed in Americlear and coverslipped with Permount. Mossy fiber sprouting was scored by a blinded observer, using a light microscope, by the criteria of Cavazos (9). Timm staining with combined immunofluorescence histochemistry was carried out according to Moos (40), using a polyclonal rabbit anti-PARP (H-250) Ab (1:50, Santa Cruz Biotechnology).

Quantitative morphometry. Numbers of zinc-positive and zinc-negative granule cell neurons, and numbers of granule cells with degenerative nuclear morphology were determined in hippocampal sections from 4-week NBD (n = 4) and control rats (n = 4). Degenerating neurons with intact but pyknotic nuclei or with nuclear/chromatin fragmentation were identified in Timm stained sections (development time = 45 minutes, longer development times resulted in intense granule cell staining, obscuring nuclear morphology) subjected to cresyl violet counterstaining. Approximately 700 granule cells per dentate gyrus, from the dorsal and ventral blades as well as the dorsal/ventral junction were analyzed per section at 100× magnification for zinc status and neurodegenerative morphology.

Statistical analysis. Data are presented as mean ± SEM. The significance of observed differences among NBD and control groups were assessed by: paired t-test for microarray experiments; ANOVA for real-time PCR analysis and quantitative morphometric analysis of zinc filled granule cells; and repeated measures ANOVA, Student t-test (non-paired data), and nonparametric statistics (Mann Whitney U test) for Timm scoring. Analysis was carried out using StatView software (v.5.0.1, SAS Institute Inc., Cary, NC). P-values were considered to be significant when <0.05.

RESULTS

Induction of MT-I/-II mRNA and protein expression in NBD rat brain. Borna disease in infected immunocompetent adult Lewis rats is mediated by infiltrating T-cells (42). In contrast, brain damage in neonatal infection occurs without overt immune cell infiltration (25). To investigate potential mechanisms of damage in neonatal infection we assessed brain mRNA expression profiles in NBD and control rats using oligonucleotide microarrays representing 8064 different gene targets. An age of 4 weeks was chosen for assessments as it correlates temporally with early histopathologic changes in dentate gyrus and cerebellum (25).

Microarray analysis of cerebellar gene expression revealed a 9.09-fold increase (p = 0.0038, paired t-test) for MT-I/-II mRNA in NBD rats, the largest fold change of any gene on the array. Hippocampal array analysis revealed a significant 2.95-fold increase in MT-I/-II (p = 0.02, paired t-test, data not shown).

A real time PCR assay was established to quantitate regional expression of MT-I/-II and MT-III mRNA in RNA extracted from individual NBD and control rat brains. Porphobilinogen deaminase mRNA served as normalization control for transcript quantity and integrity. NBD rats had marked increases in MT-I/-II mRNA in cerebellum (40.5-fold, p<0.0001), hippocampus (6.8-fold, p = 0.003), and striatum (9.5-fold,

p = 0.0012) (Figure 1A, B, C). Western immunoblot analysis was employed to assess levels of MT-I and MT-II expression in extracts of NBD and control rat brain (Figure 1D). MT-I (14-kDa bands) and MT-II (11-kDa bands) were increased in NBD cerebellum and striatum; in NBD hippocampus, MT-II was predominantly increased. While not significant, real-time PCR for MT-III revealed a trend toward decreased MT-III in hippocampus (1.25-fold, p = 0.0841) (Figure 1A).

Regional expression of MT-I/-II was assessed in brain sections of 4-week-old NBD and control rats by immunofluorescence microscopy. MT-I/-II expression was increased in NBD rats with striking immunoreactivity in cerebellum in proximity to Purkinje cells (Figure 2B, C), in molecular layer of dentate gyrus (Figure 2E, F) and in corpus callosum (Figure 2H, I). MT-I/-II induction was also present in cells with glial morphology in the stratum-lacunosum moleculare, stratum radiatum, and stratum oriens of hippocampus; caudate-putamen; and cortex of NBD rats (data not shown). Only faint immunoreactivity was present in control rat hippocampus (Figure 2D) and corpus callosum (Figure 2H); no immunoreactivity was observed in control cerebellum (Figure 2A).

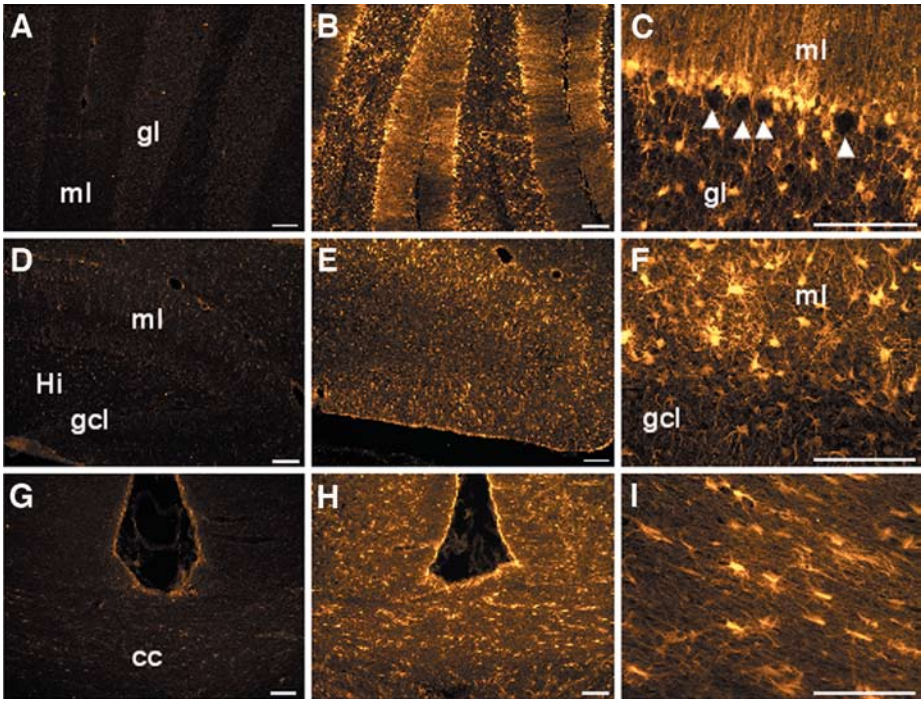

Figure 2. *Localization of increased MT-I/-II expression in NBD rat brain.* MT-I/-II in cerebellum (**A, B, C**), dentate gyrus (**D, E, F**), and corpus callosum at the level of striatum (**G, H, I**) in control rats (**A, D, G**) and NBD rats (**B, C, E, F, H, I**). Purkinje cells are indicated by white arrow heads (**C**). Molecular layer, ml; granular layer, gl; granule cell layer, gcl; hilus, Hi; corpus callosum, cc. Immunofluorescence using a mouse monoclonal antibody to horse MT-I/-II and anti mouse IgG Cy3. Scale bars = 100 μm.

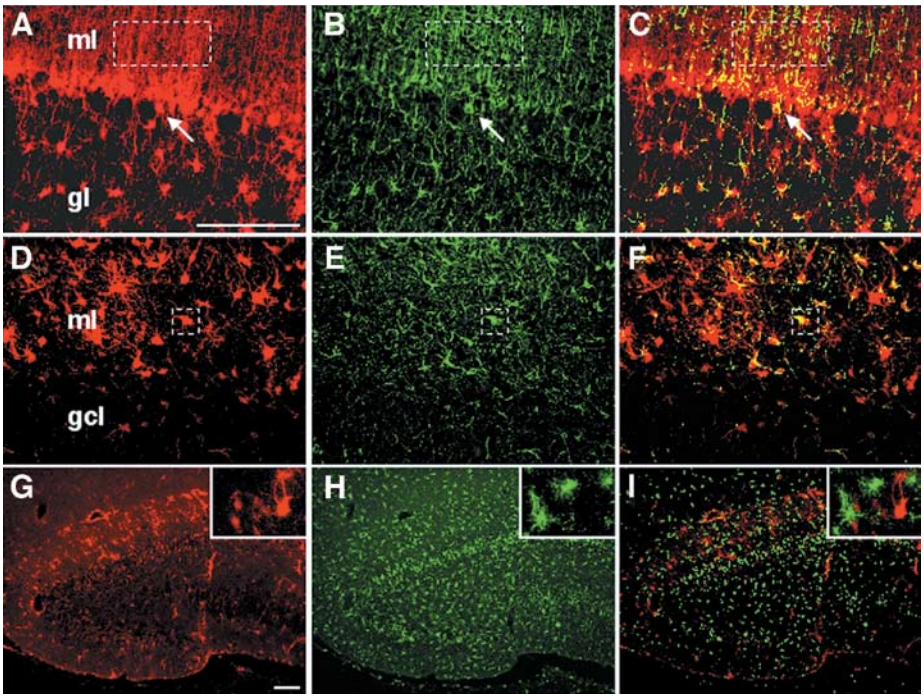

Figure 3. *Colocalization of MT-I/-II with astrocytes but not microglia in NBD rat brain.* Double immunofluorescence for MT-I/-II (**A**, red) and GFAP (**B**, green) in the cerebellum. Merged image (**C**) shows colocalization (yellow) within cells lining the Purkinje cell layer (arrow) as well as Bergmann fibers (boxed region) in the molecular layer. MT-I/-II (**D**) and GFAP (**E**) double staining (merged in **F**) in the molecular layer of the dentate gyrus. MT-I/-II (**G**) and Iba1 (**H**, microglia) double staining in the dentate gyrus. Note that MT-I/-II and Iba1 colocalization does not appear in the merged image (**I**, insets show high magnification of glia in dentate molecular layer). Molecular layer, ml; granular layer, gl; granule cell layer, gcl. Scale bars = 100 μM.

Expression of MT-I/-II in NBD rat brain astrocytes. Prominent astrogliosis and microgliosis are reported in NBD rat brain (62). Double label immunofluorescence experiments were pursued using antibodies to MT-I/-II and markers specific for astrocytes (GFAP) or microglia (Iba1) to assess the cellular distribution of MT-I/-II. MT-I/-II colocalized with GFAP in cerebellum (Figure 3A, B, C) and hippocampus (Figure 3D, E, F), but did not colocalize with Iba1 (Figure 3G, H, I; insets show dissociation between MT-I/-II and microglia staining at higher magnification). Iba1 expression was, however, consistent with microgliosis previously described in NBD. MT-I/-II immunopositive glial cells in caudate-putamen, laminar regions of the hippocampus, and cortex also colocalized with GFAP, confirming astrocyte-specific induction of MT-I/-II in all brain regions examined (data not shown). Cerebellum was remarkable for double labeling of cells consistent in location and morphology with Bergmann glial fibers (Figure 3C; boxed area) and cell bodies (Figure 3C; arrow). Some cell bodies expressing MT-I/-II did not label with antisera to GFAP. We were unable to discern whether these represent additional special-

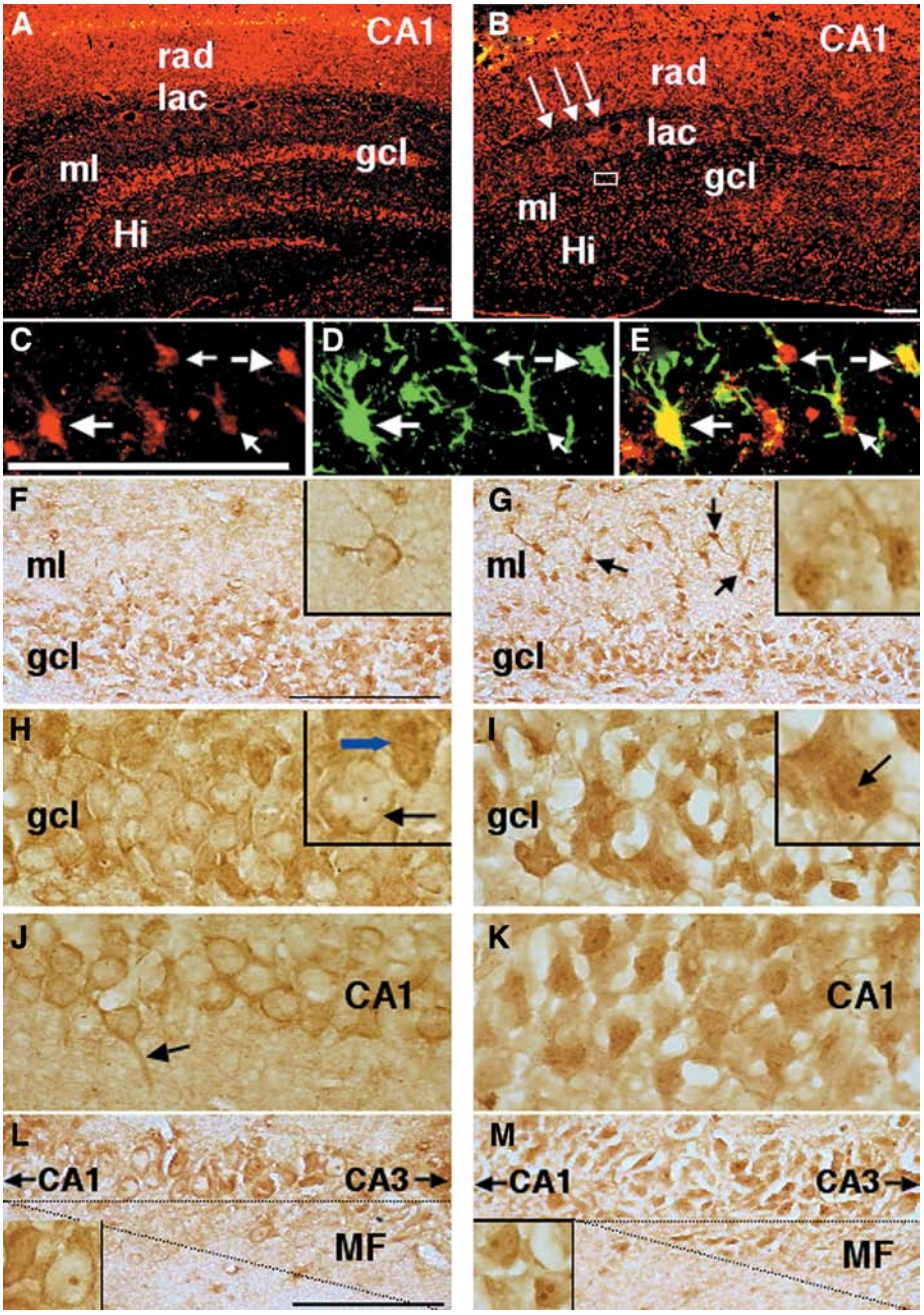

Figure 4. Localization and subcellular distribution of MT-III in hippocampal astrocytes and neurons in NBD. **A.** Immunofluorescent signal for MT-III in control rat hippocampus (note strong signal in CA1 pyramidal neurons [saturated signal in yellow] and dentate gyrus granule cell neurons). **B.** MT-III fluorescence in NBD rat hippocampus (note decreased signal in granule cell layer; arrows indicate loss of signal at the boundary of lacunosum moleculare and stratum radiatum). MT-III (**C**) and GFAP (**D**) double immunofluorescence (merged in **E**) corresponding to astrocytic signal in the molecular layer of the dentate gyrus (boxed region in **B**). Immunohistochemical staining of MT-III in the molecular layer of the dentate gyrus in control (**F**) and NBD rat (**G**, arrows indicate a few MT-III immunopositive glial cells). Note that glial staining for MT-III is dramatically increased in NBD rat and localizes to glial cell bodies, glial processes, and nucleus/nuclear bodies (inset in **G**); immunostaining is restricted to perinuclear cytoplasm and glial processes in control rats (inset in **F**). Immunohistochemical staining of dentate gyrus granule cell neurons in control (**H**) and NBD rat (**I**). Immunohistochemical staining of CA1 pyramidal neurons in control (**J**) and NBD rat (**K**). MT-III staining at the CA3-CA1 boundary of control (**L**) and NBD rat (**M**). Abbreviations: rad, stratum radiatum; lac, stratum lacunosum-moleculare; ml, molecular layer of the fasciae dentate; Hi, hilus fasciae dentate; gcl, granule cell layer; CA1, stratum pyramidale of CA1 subregion; MF, mossy fibers. Scale bars = 100 µm.

ized cells in the cerebellum, such as basket cells or stellate cells adjacent to Purkinje cells, or restricted GFAP expression in some astrocytes.

Alterations in MT-III protein expression and subcellular distribution in hippocampal astrocytes and neurons in NBD rats. High levels of MT-III have been localized to neurons that contain vesicular zinc in the hippocampus (38), where it has been suggested that MT-III may serve as a source of intracellular zinc that mediates neuronal death (34). Real-time PCR analysis (see above) suggested that MT-III mRNA may be decreased in the hippocampus of NBD rats. Thus, we assessed the cellular distribution of MT-III protein in NBD and control rats by immunofluorescence and immunohistochemistry.

MT-III fluorescence in control rats was consistent with previous reports localizing MT-III to neurons. The intensity of neuronal immunoreactivity for MT-III in control rat hippocampus was high in CA1 pyramidal (saturated signal in Figure 4A) and granule cell neurons, and lower in CA3 pyramidal neurons. Laminar fluorescence was intense in the CA1 subregion of the stratum radiatum, with only weak staining in neuropil of the stratum lacunosum moleculare, CA3 subregion of stratum radiatum, the molecular layer of the dentate gyrus, and hilus (Figure 4A)

In NBD MT-III was reduced in the granule cell layer, CA1 pyramidal neurons, and in the stratum radiatum but increased in stratum lacunosum moleculare. A clear zone of MT-III loss was observed at the laminar interface between stratum radiatum and stratum lacunosum moleculare in NBD rats (Figure 4B; arrows), which may represent loss of MT-III in axons of the perforant path.

Strong MT-III fluorescence was observed in numerous astrocytes in NBD hippocampus (Figure 4C, D, E correspond to the boxed region in Figure 4B), whereas, only small numbers of weakly positive astrocytes were observed in control rats. MT-III appeared to primarily stain astrocyte cell bodies (Figure 4C; arrows), with less intense staining in glial processes. GFAP localized to cell bodies (Figure 4D; large arrow) and processes (Figure 4D; small arrows) of MT-III positive astrocytes (merged in Figure 4E). Immunohistochemical analysis of MT-III confirmed increased astrocytic MT-III staining in the molecular layer of the dentate gyrus (Figure 4G; arrows), stratum radiatum, stratum lacunosum moleculare, hilus, and cortex (not shown). In control

rats, faint immunostaining was observed in the perinuclear cytoplasm and processes of astrocytes; whereas staining was completely excluded from the nucleus (Figure 4F; inset). In contrast, in NBD rats, MT-III staining was prominent in astrocytic nuclei, nuclear bodies, and glial processes (Figure 4G; inset).

Immunohistochemical staining patterns in dentate gyrus granule cell neurons of control rats revealed that the majority of MT-III localized to the perinuclear cytoplasm (Figure 4H; inset black arrow); however, nuclear MT-III was observed in a few granule cell neurons in control rats (Figure 4H; inset blue arrow). In NBD rats, MT-III staining of granule cell neuronal nuclei and nuclear bodies was prominent throughout the dentate gyrus (Figure 4I; inset).

In control rat CA1 pyramidal neurons, where MT-III signal is strongest, staining was strictly cytoplasmic and evident in axons of pyramidal neurons extending into stratum radiatum (Figure 4J; arrow). Similar to NBD granule cell neurons, CA1 pyramidal neurons in NBD exhibited strong MT-III immunostaining, largely localized to nuclei and nuclear bodies (Figure 4K).

The only neurons in the hippocampus of control rats showing prominent localization in nuclear bodies were found at the boundary of CA3-CA1/CA2 pyramidal neurons where mossy fibers terminate. Here MT-III was primarily restricted from the nucleus, but was apparent in perinuclear cytoplasm as well as nuclear bodies (Figure 4L; inset). In NBD rat pyramidal neurons at the CA3-CA1 boundary, MT-III immunostaining was present in both nucleus and nuclear bodies (Figure 4M; inset). In contrast to other neurons in the hippocampus, the remainder of CA3 pyramidal neurons extending from the hilus to the CA3-CA1 boundary showed nuclear MT-III staining in both control and NBD rats (not shown).

The MT-III antibody stained mossy fibers, only faintly, in both control and NBD rats and was most prominent at the CA3-CA1 boundary (outlined region in Figure 4L, M). Though there appeared to be a general thinning of the mossy fiber layer in NBD rats compared to controls, staining intensity appeared similar.

Outside the hippocampus, MT-III was seen in cortical and thalamic neurons, where staining was similar between control and NBD rats. In these neurons, MT-III was observed in perinuclear cytoplasm, nucleus, nuclear bodies, and axons (data not shown).

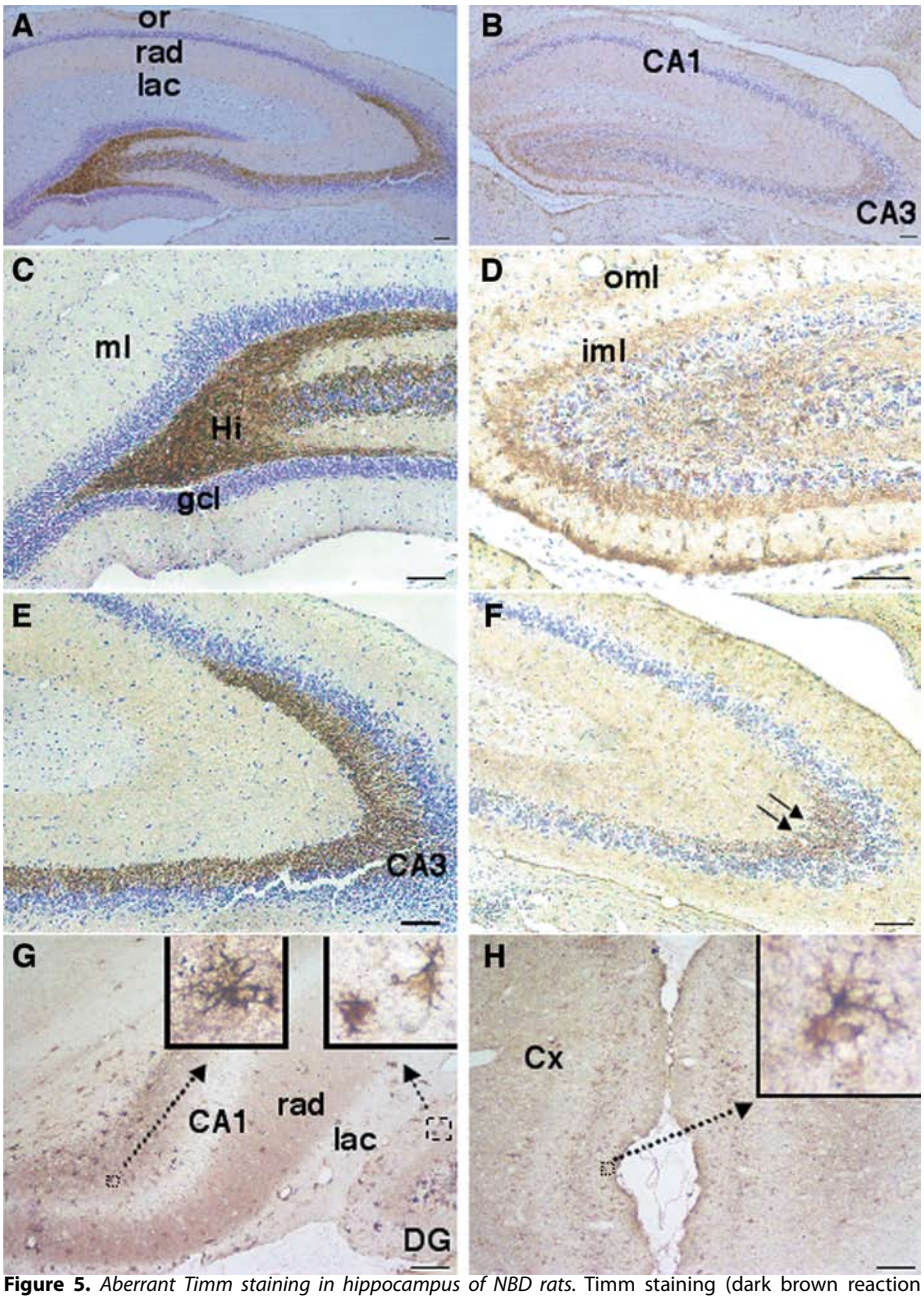

Figure 5. *Aberrant Timm staining in hippocampus of NBD rats.* Timm staining (dark brown reaction product) in control (**A, C, E**) and NBD rats (**B, D, F, G, H**). Note decreased zinc in the hilus (**D**) and sector CA3 (**F**) of NBD rats. Arrows in (**F**) indicate decreased staining in mossy fiber projections to CA3. Zinc staining in glial cells in NBD rats (**G, H**). Glial staining was absent from control rats (data not shown). Zinc accumulation in glial cells from the dentate gyrus molecular layer (**G**, right inset), and stratum oriens in CA1 sector (**G**, left inset). Zinc stained glial cells in cortex of NBD rat (**H**). Abbreviations: or, stratum oriens; rad, stratum radiatum; lac, stratum lacunosum-moleculare; ml, molecular layer of the fasciae dentate; Hi, hilus fasciae dentate; gcl, granule cell layer; iml, inner molecular layer; oml, outer molecular layer; Cx, cortex. Scale bars = 100 µm.

Reduced zinc in granule cell mossy fibers and accumulation of zinc in glial cells in NBD rat hippocampus. A modified Timm stain (dark brown reaction product) was used to examine the level and distribution of zinc in NBD and control rat brains. In control rats, zinc signal was intense and confined to mossy fiber projections in the hilus (Figure 5A, C) and CA3 (Figure 5A, E). In NBD, histochemically detectable zinc was dramatically reduced in mossy fiber processes in the hilus (Figure 5B, D) and CA3 (Figure 5B, F; arrows). Glial cells in NBD, but not in control rats, stained strongly for zinc, though glial staining was only evident when counterstaining was

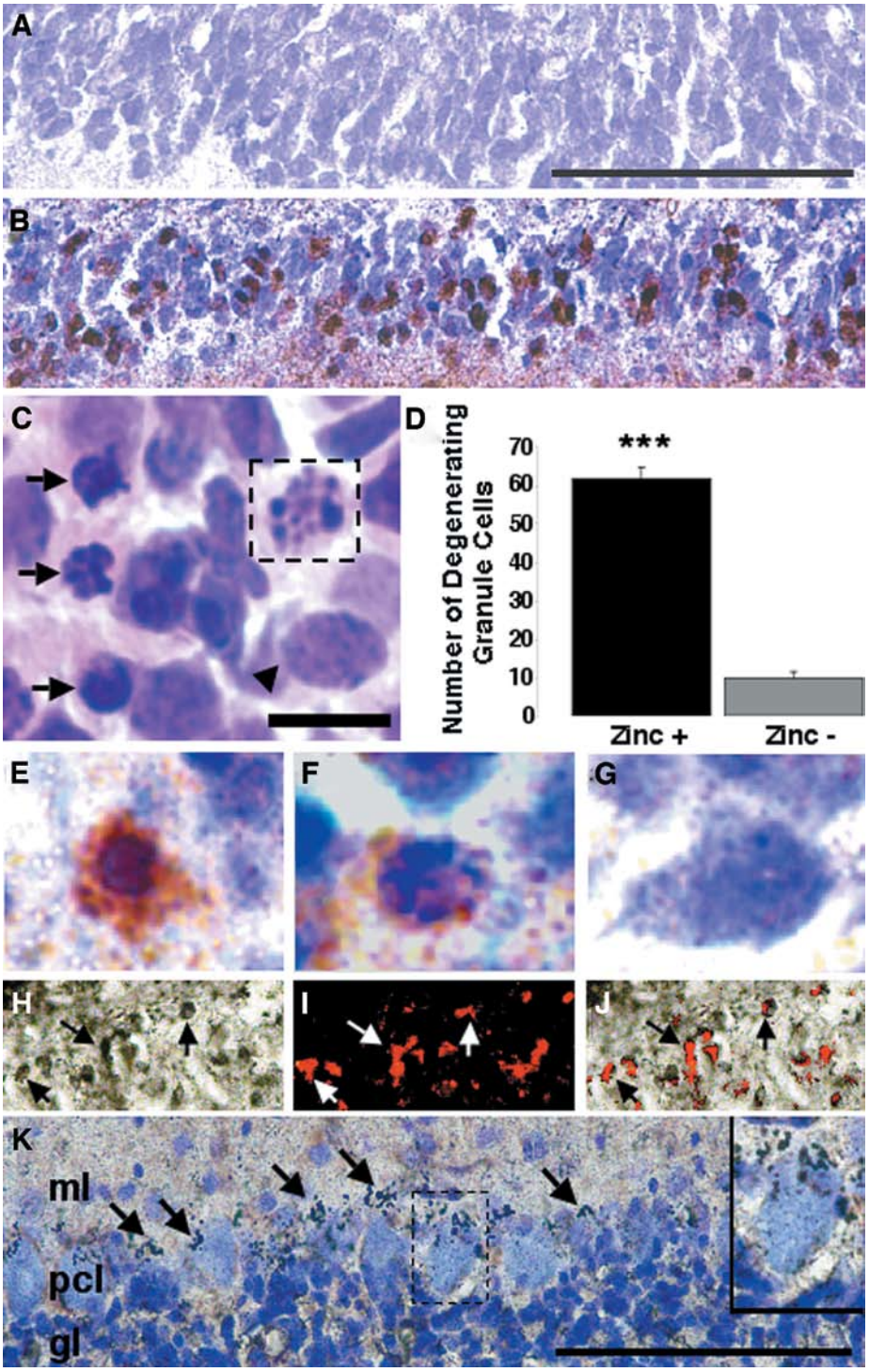

Figure 6. *Zinc accumulation in degenerating granule cell neurons in NBD rats.* **A.** Timm staining is absent in control granule cell neurons. **B.** Numerous Timm positive granule cell somata in NBD rats. **C.** H&E staining of degenerative dentate gyrus granule cells in NBD, showing different morphology of nuclei in these cells (arrow head indicates neuron with normal morphology, arrows indicate neurons with intact, pyknotic nuclei, boxed cell shows clear signs of nuclear/chromatin fragmentation). **D.** Bar plot representing quantitative morphometric analysis of zinc-positive and zinc-negative degenerating granule cell neurons in NBD rats. Data are presented as mean score ± SEM (n = 4 NBD rat hippocampi) (86% of all neurons with degenerative morphology were Timm positive: ANOVA, $p<0.0001$). **E.** Granule cell neuron with distinct nuclear pyknosis and cytoplasmic zinc accumulation (brown product). **F.** Granule cell neuron with conspicuous nuclear/chromatin fragmentation, and cytoplasmic zinc accumulation. **G.** Morphologically normal neuron from Timm stained NBD rat section, counterstained with cresyl violet. **H, I, J.** Colocalization of Timm stain and PARP in dentate gyrus granule cells in NBD. **H.** Timm stain; (**I**) PARP immunofluorescence; (**J**) superimposition of panels (**H**) and (**I**). **K.** Timm stained cerebellar section from NBD rat. Note the lack of zinc in Purkinje cell neurons, and presence of granular zinc staining lining the Purkinje cell layer. No differences in zinc staining intensity or localization were observed in cerebellum between control and NBD rats. Triple asterisk indicates $p<0.0001$ relative to control (ANOVA). Abbreviations: ml, molecular layer of the cerebellum; pcl, Purkinje cell layer; gl, granule cell layer of cerebellum. Scale bar = 10 µm for (**C**); Scale bars = 100 µm for (**A, K**).

omitted. Morphologically, glial cells resembled reactive astrocytes and paralleled the distribution of metallothionein-positive astrocytes. Zinc-positive glia localized to the molecular layer of the dentate gyrus (Figure 5G; right inset); stratum lacunosum moleculare, stratum radiatum, and stratum oriens (Figure 5G; left inset); dorsal hippocampal commissure; corpus callosum; and cortex (Figure 5H).

Accumulation of zinc in degenerating granule cell somata in NBD rat hippocampus. Granule cell staining was completely absent in control animals (Figure 6A). In NBD rats, Timm stained granule cell bodies were strongly zinc-positive (Figure 6B). Hematoxylin and eosin staining revealed neurons in NBD rats with intact, but pyknotic nuclei (Figure 6C; arrows) or nuclear/chromatin fragmentation (Figure 6C; boxed cell). These degenerative morphological changes were observed in approximately 10% of all granule cell neurons in 4-week NBD rats; none of the neurons in control animals exhibited signs of neurodegeneration. With relatively short Timm development time (45 minutes), and counterstaining with cresyl violet, morphological examination revealed that all zinc-positive granule cell neurons showed prominent signs of neurodegeneration. Zinc was present in most granule cells with pyknotic nuclei (Figure 6E) and morphological signs of nuclear/chromatin fragmentation (Figure 6F). In contrast, morphologically normal neurons without evidence of pyknosis or nuclear fragmentation were never zinc-positive, even in NBD rats (Figure 6G). The subset of zinc-positive neurons with morphological signs of neurodegeneration (either pyknosis or nuclear/chromatin fragmentation) in NBD represented 86% (61.75 ± 3.07) of all neurons with neurodegenerative morphology, compared to 14% (9.75 ± 1.80) of degenerating neurons that were zinc-negative (Figure 6D; zinc-positive degenerating neurons versus zinc-negative degenerating neurons: ANOVA, $p<0.0001$). The find-

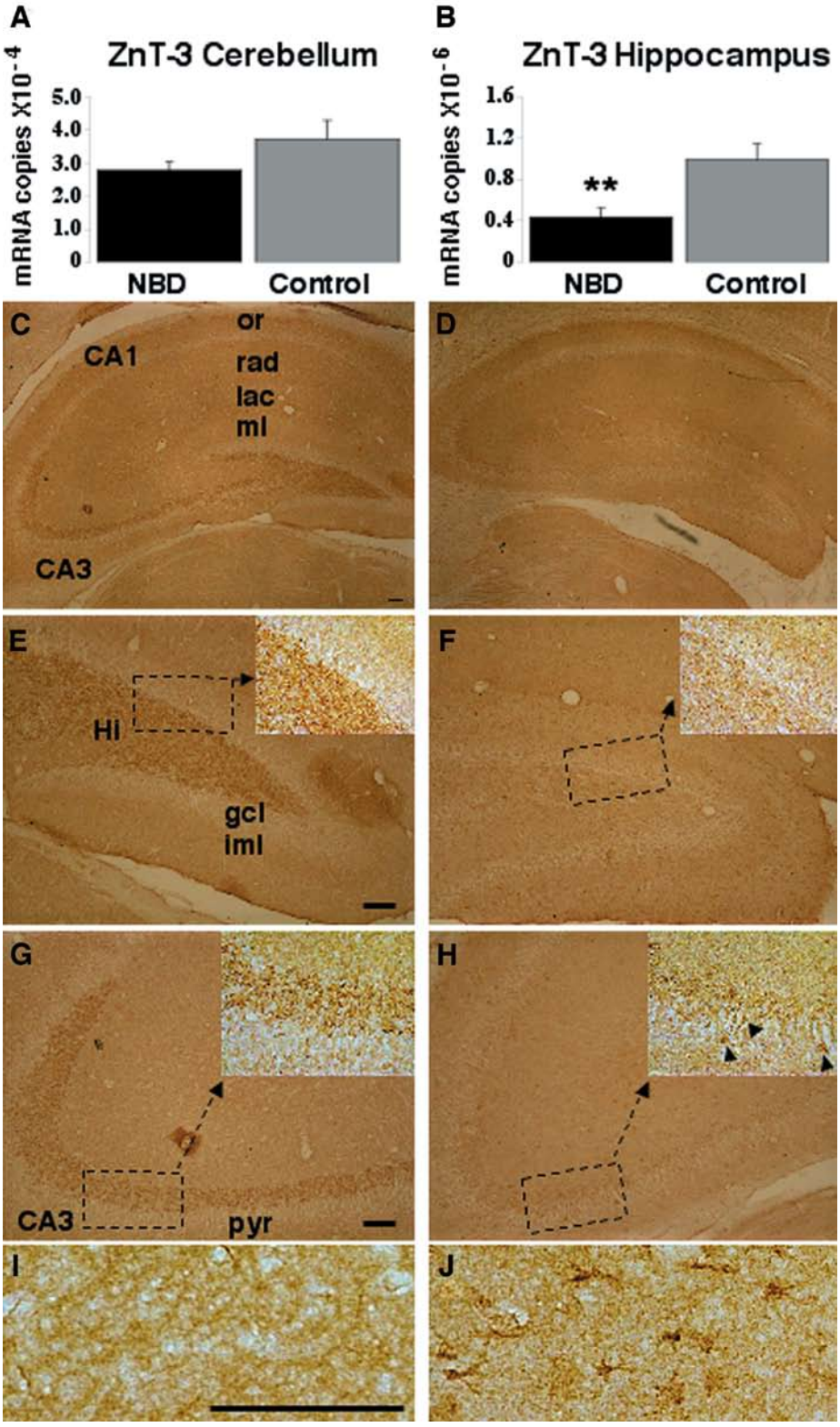

Figure 7. *ZnT-3 mRNA and protein are decreased in NBD hippocampal mossy fibers.* **A.** ZnT-3 mRNA in cerebellum of NBD (n = 7) and control (n = 5) rats (1.3-fold decrease in NBD rat mRNA relative to control rats: ANOVA, p = 0.1249). **B.** ZnT-3 mRNA in NBD rat hippocampus; NBD (n = 7) and control (n = 5); (2.27-fold decrease in NBD rats: ANOVA, p = 0.0065). ZnT-3 immunoreactivity in transverse sections of control (n = 4) (**C, E, G, I**) and NBD (n = 4) (**D, F, H, J**) rat hippocampus reacted with affinity-purified antiserum against ZnT-3. **C, D.** ZnT-3 protein is decreased throughout the mossy fiber projections from granule cells to CA3 in NBD rats. **E, F**. Strong immunoreactivity is evident in the hilus of control animals, while staining is virtually undetectable in NBD rats. **G, H.** ZnT-3 staining of mossy fibers projecting to CA3 are dramatically reduced in NBD rats. Note ZnT-3 staining in pyramidal neurons of CA3 (arrow heads in **H** inset). **I, J.** At higher magnification, glial cells in the molecular layer of the dentate gyrus of NBD rats are ZnT-3 immunopositive. Double asterisk indicates p<0.01 relative to control rats (ANOVA). Abbreviations: or, stratum oriens; rad, stratum radiatum; lac, stratum lacunosum-moleculare; ml, molecular layer of the fasciae dentate; Hi, hilus fasciae dentate; gcl, granule cell layer; iml, inner molecular layer; pyr, stratum pyramidale. Scale bars = 100 µm.

ing that a small number of degenerating neurons were zinc-negative may suggest that a subset of degenerating neurons are not associated with alterations in zinc or that zinc accumulation is dependent on the stage of neurodegeneration. Alternatively, we cannot exclude the possibility that these neurons would become zinc-positive with longer Timm development time. However, an evaluation of the mean number of zinc-positive neurons in serial sections with 90-minute Timm development (72 ± 6.35) showed values nearly identical to the total number of neurons with degenerative morphology (71.5 ± 4.56) (45-minute Timm development: zinc-positive + zinc-negative from Figure 6D).

Overactivation of the DNA repair enzyme poly(ADP-ribose) polymerase (PARP) has been implicated in zinc-induced cell death (51). Increased PARP mRNA has been localized to dentate gyrus in models of ischemic and excitotoxic insult (37). We have evaluated PARP protein expression in NBD and control rats using combined Timm staining and immunofluorescence histochemistry. In control rats, low levels of PARP immunoreactivity were uniform throughout the granule cell layer (data not shown). In contrast, in NBD rats, Timm stained granule cells (Figure 6H) colocalized with cells exhibiting strong PARP signal (Figure 6I; merged in Figure 6J). PARP immunofluorescence in non-Timm stained tissues revealed similar increases in PARP immunoreactivity in the dentate gyrus (data not shown).

As Purkinje neurons are also lost in NBD rats, we utilized the Timm technique in cerebellar sections. Purkinje cell neurons did not appear to accumulate zinc in NBD rats. Zinc staining was remarkably similar between NBD and control rats in all sections analyzed. Interestingly, although Timm granules were not observed in the somata of Purkinje neurons, we observed staining

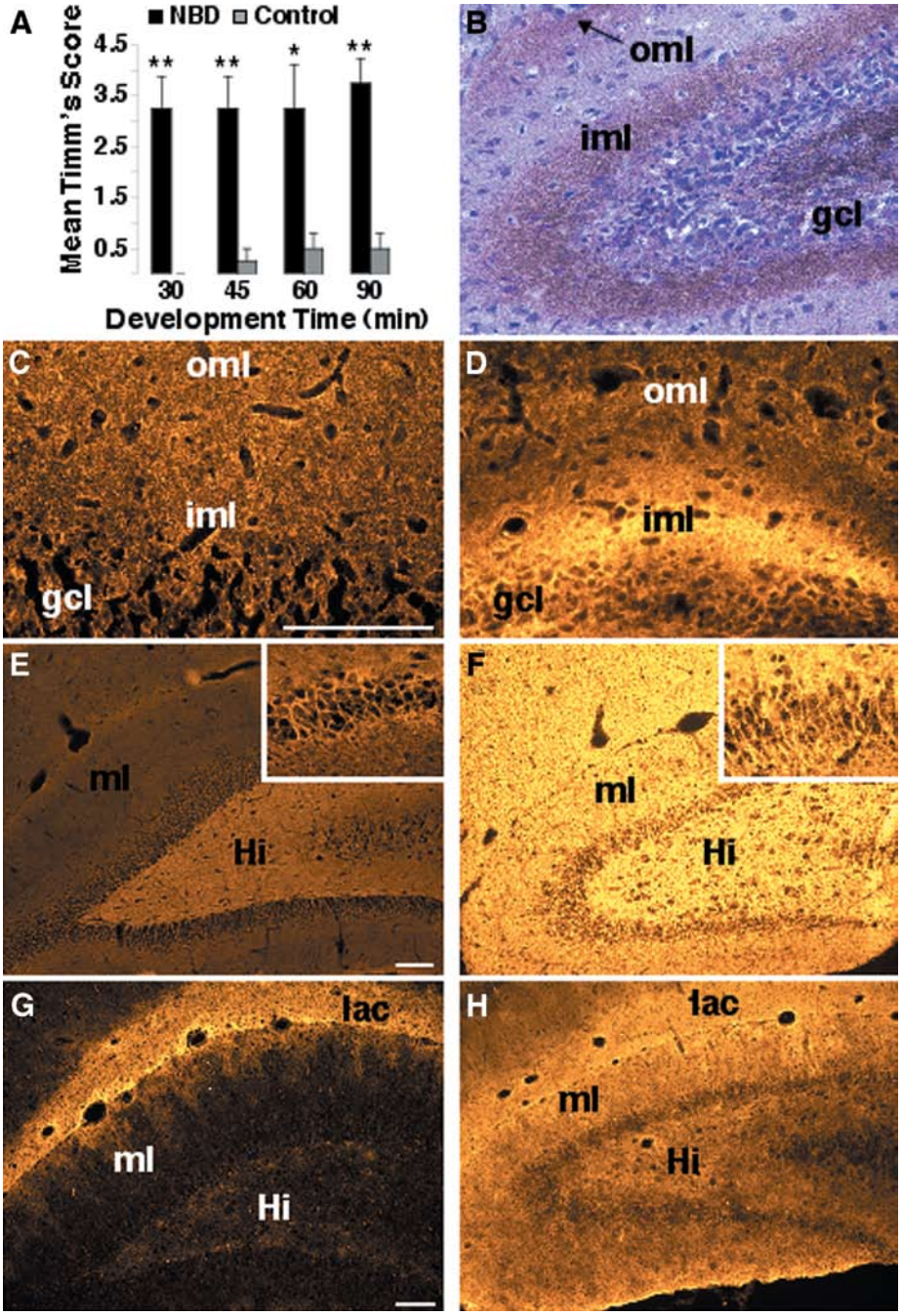

Figure 8. *Mossy Fiber Sprouting in NBD rat hippocampus.* **A.** Bar plot representing Timm scores in NBD and control rats at different development times as described in Methods. Data are presented as mean score ± SEM [Repeated measures ANOVA: $p = 0.0033$; Mann Whitney Comparison: $p < 0.0001$; Unpaired t-test 30min: $p = 0.0021$; Unpaired t-test 45min: $p = 0.0044$; Unpaired t-test 60 minutes: $p = 0.0225$; Unpaired t-test 90 minutes: $p = 0.0011$]. **B.** Timm staining in the inner and outer molecular layer of the dentate gyrus in NBD rats. **C.** Synaptophysin immunoreactivity in dentate molecular layer of control rat. **D.** Synaptophysin immunoreactivity in dentate molecular layer of NBD rat. **E.** Tenascin-R (TN-R) immunoreactivity in control rat dentate gyrus shows moderate fluorescence in neuropil of the hilus and weak fluorescence in the inner molecular layer. (Inset in **E**) TN-R immunoreactivity in CA3 pyramidal cell layer of control rats with well-defined fluorescence in perineuronal nets and weak fluorescence in neuropil. **F.** TN-R immunofluorescence in NBD rat dentate gyrus. Note the homogeneous increase in TN-R fluorescence in the neuropil. (inset in **F**) Strong TN-R immunoreactivity in neuropil surrounding CA3 pyramidal neurons in NBD rats. **G.** CD44 immunoreactivity in the dentate gyrus of control rat. **H.** Dentate gyrus of NBD rat, showing increased CD44 fluorescence in the neuropil of the molecular layer and hilus. Asterisk indicates $p < 0.05$; double asterisk indicates $p < 0.01$ relative to control rats (Unpaired student t-test). Abbreviations: Molecular layer, ml; granule cell layer, gcl; hilus, Hi; inner molecular layer, iml; outer molecular layer; oml; stratum lacunosum-moleculare, lac. Scale bar = 100 µm.

in close apposition to the Purkinje cell layer in both NBD (Figure 6K) and control rats.

Zinc transporter mRNA and protein expression in NBD rat brain. Zinc transporters contribute to zinc homeostasis and bioavailability via mechanisms of storage and release. Additionally, zinc and other heavy metals induce MT expression, and MT participates in regulation of zinc homeostasis and bioavailability. To assess the role aberrant zinc transporter expression may play in zinc and MT dysregulation, we established real time PCR assays for quantitation of mRNA encoding ZnT-1 and ZnT-3. No differences were observed between NBD and control rats with respect to ZnT-1 mRNA levels in either hippocampus or cerebellum (data not shown). In contrast, ZnT-3 mRNA was significantly decreased in the hippocampus of NBD rats (2.27-fold, $p = 0.0065$) (Figure 7B). ZnT-3 mRNA levels did not differ in cerebellum of NBD and control rats (Figure 7A).

The distribution of ZnT-3 in hippocampus was assessed immunohistochemically in NBD and control rats. ZnT-3 immunoreactivity in control rats was concentrated at points where granule cell mossy fiber boutons make contact with hilar neurons (Figure 7E) and pyramidal cells of CA3 (Figure 7G; inset), consistent with previous reports (43). In NBD rats, in contrast, ZnT-3 was markedly reduced or undetectable in mossy fiber projections (Figure 7D, F, H). Occasional immunopositivity was observed in somata of pyramidal neurons in CA3 of NBD rats, but not in controls (Figure 7H; inset, arrowheads). ZnT-3 immunopositive cells with glial morphology were not observed in control rats (Figure 7I) but were present throughout the molecular layer of the dentate gyrus and the stratum lacunosum moleculare and stratum radiatum in NBD rats (Figure 7J).

Mossy fiber sprouting in NBD rats. The potential effects of neural injury on mossy fiber sprouting (MFS) were examined by using Timm stain. Timm MFS scores revealed marked increases in zinc reactivity in the inner molecular layer of the dentate gyrus of all 4 NBD rats compared to controls, irrespective of development time (Figure 8A). Timm staining is not strictly quantitative, as it is dependent on perfusion efficiency; nonetheless, even with develop-

ment times as long as 90 minutes, MFS was never observed in control animals. Robust MFS into the inner molecular layer was observed in NBD; Timm reaction was also pronounced in the outer molecular layer of NBD rats (Figures 5D, 8B). In other brain regions (ie, cerebellum, striatum, cortex), Timm reaction intensity was similar in NBD and control rats. As an independent assay for mossy fiber sprouting we pursued synaptophysin immunostaining in the brains of 4-week-old NBD rats. Reactivity of synaptophysin is considered a reliable index for synaptic density, and increased synaptophysin has previously been demonstrated in NBD rats in the inner molecular layer of the dentate gyrus (22). Synaptophysin immunofluorescence paralleled the spatial distribution of zinc in mossy fibers observed with Timm staining. Compared to control rats (Figure 8C), synaptophysin is dramatically increased in NBD rats in the inner molecular layer (Figure 8D), but decreased in the hilus and mossy fiber projections to CA3 (data not shown).

Distribution of extracellular matrix glycoproteins implicated in mossy fiber sprouting. Hippocampal expression of the extracellular matrix glycoprotein molecules, tenascin-R (TN-R), and the hyaluronan receptor, CD44, is implicated in the development of MFS in other animal model paradigms (4, 5). Thus, we examined the distribution of these proteins in NBD. In control rats, TN-R immunoreactivity was restricted to the hilar neuropil (Figure 8E) and perineuronal nets surrounding pyramidal neurons (Figure 8E; inset) of the CA regions. In NBD rats, TN-R and CD44 expression were increased throughout the hippocampal neuropil (Figure 8F and H, respectively). TN-R fluorescence in CA3 neuropil of NBD rats was so intense that the presence or absence of expected patterns of immunoreactivity in the perineuronal nets surrounding pyramidal neurons could not be evaluated (Figure 8F; inset). CD44 expression in control rats was seen primarily in neuropil of stratum lacunosum-moleculare, with faint immunoreactivity in the outer molecular layer and hilus (Figure 8G).

DISCUSSION

Here, we report altered expression of genes regulating zinc homeostasis in a model of virus-induced neurodevelopmental damage. To our knowledge, these findings represent the first demonstration in brain of significant MT-I/-II and MT-III induction with disrupted zinc regulatory systems in response to perinatal viral infection. We provide evidence of altered zinc distribution in hippocampus, suggesting that selective zinc-mediated toxicity may contribute to apoptotic losses of dentate gyrus granule cells and to specific neuroplastic changes in zinc-enriched mossy fibers in hippocampus. The experiments of this study demonstrate significant alterations in zinc regulation in NBD rats, including: *i)* induction of metallothioneins I, II, and III in astrocytes, *ii)* loss and altered subcellular distribution of MT-III in hippocampal neurons, *iii)* redistribution of zinc from mossy fiber boutons to somata of degenerating neurons, *iv)* loss of vesicular zinc sequestering capacity through disrupted ZnT-3 expression, and *v)* aberrant reorganization of zinc-enriched, excitatory synaptic circuits.

Metallothioneins (MT) are low-molecular weight, cysteine-rich, intracellular metal-binding proteins found in a wide variety of organisms including bacteria, fungi, plants and animals. The MT-I and MT-II isoforms are ubiquitously expressed and coordinately regulated. Expression of MT-I/-II is induced by heavy metals (eg, zinc, copper, mercury, cadmium, and nickel), glucocorticoids, proinflammatory cytokines, and oxidative stress-inducing agents (16). Studies in knockout mice have ascribed functional properties to metallothionein, including protection against toxicity from heavy metals and other xenobiotics such as carbon tetrachloride (31, 32). In NBD rats, MT-I/-II is readily detected in reactive astrocytes in cerebellum and hippocampus. Induction of MT-I/-II expression has been described in peripheral tissues in other rodent viral infection models, notably influenza A virus infection (liver and lung), and coxsackie B infection (liver, kidney, spleen) (21, 27). In addition to zinc regulatory effects on MT-I/-II mRNA and protein, infection nonspecifically increases proinflammatory cytokines and glucocorticoids, factors that can also strongly induce MT-I/-II expression. In this context it is intriguing that mRNA for cytokines implicated in metallothionein synthesis during inflammatory states, such as IL-1, IL-6 and TNF-α, are increased in NBD rat brains at 4 weeks, the time point examined here (25, 48). The cellular distribution of MT-I/-II immunoreactivity in NBD rat brain in astrocytes is consistent with that observed in other models of neural injury and CNS toxicity (24). MT-I and MT-II are reported to be coordinately regulated (65); thus, the regional differences we observed in MT-I and MT-II expression in NBD rats were not anticipated. Whereas MT-I and MT-II were expressed in the cerebellum and striatum at similar levels, levels of MT-II were higher than MT-I in hippocampus. A potential explanation for discordance may be found in the observation that some cytokines can cause variation in MT isoform expression in peripheral organs; eg, IL-6 and TNF-alpha induce more MT-II than MT-I in the liver (47). Thus, inductive mechanisms or posttranscriptional regulation by cytokines may be regionally disparate in the brains of NBD rats.

MT-III expression is confined primarily to the CNS. MT-III is believed to be less sensitive to induction than either MT-I or MT-II. Originally named growth inhibitory factor because it decreased survival of neonatal rat cortical neurons, MT-III is concentrated in neurons, especially glutamatergic neurons in hippocampus, where zinc is sequestered in synaptic vesicles (38, 58). In these neurons, MT-III may exert protective effects against zinc toxicity and oxidative damage, or mediate zinc transport to synaptic vesicles. MT-III inhibits regenerative neurite sprouting in cortical neurons following axonal damage; its deficiency is proposed to contribute to abnormal sprouting patterns in Alzheimer disease (eg, neurofibrillary tangles) and epilepsy (14). Additionally, studies in *Mt3*-null mice provide evidence that MT-III may serve as an intracellular zinc source, contributing to neuronal zinc toxicity following kainate-induced seizures (34). We found only a trend toward decreased MT-III mRNA in the hippocampus of NBD rats at 4 weeks. Immunohistochemical analysis of MT-III revealed decreased immunostaining in the dentate gyrus granule cell layer (likely attributable to granule cell degeneration) and increased astrocytic expression in NBD hippocampus. The differential cellular expression of MT-III likely explains our lack of significant findings for MT-III at the mRNA level, as these would depend on both the level of granule cell damage

(leading to an anticipated MT-III mRNA decrease) and astrocytic MT-III induction (leading to an anticipated MT-III mRNA increase); the balance of such processes may vary in individual NBD rats. Increased glial MT-III expression has been demonstrated in other brain injury models, and in vitro results suggest that MT-III may promote astrocyte migration (7). In zinc-enriched hippocampal neurons, MT-III may operate as a concentrated, vital sink for unbound zinc (2). Thus, loss of MT-III in granule cell neurons could have neuropathological consequences, resulting in accumulation of neurotoxic levels of free zinc. In control rats MT-III appears to be primarily cytoplasmic in dentate gyrus granule cell neurons and CA1 pyramidal neurons. Redistribution in NBD rats of MT-III to the nucleus of granule cells in dentate gyrus, where large amounts of histochemically detectable zinc are found in mossy fibers, could result in sequestration of MT-III's zinc buffering capacity from the cytoplasm, allowing for the accumulation of excessive cytoplasmic free zinc. Neuroprotective effects in vitro have been demonstrated for MT-III against glutamate, nitric oxide, β-amyloid peptide 25-35, S-nitrosothiols and H_2O_2 (8). In addition to MT-I/-II, MT-III has been confirmed, in vitro, to be protective against hydroxyl radical-induced DNA single-strand breaks and deoxyribose degradation (67). In protecting against oxidative damage, MT-III may release zinc when its sulfhydryl residues become oxidized, thus contributing to increased intracellular free zinc concentrations (17). Our findings of subcellular redistribution of MT-III from perinuclear cytoplasm in normal rat to nucleus/nuclear bodies in NBD rat hippocampal neurons and astrocytes may add credence to a proposed role for MT-III in protecting against genotoxic stress. Nuclear import/retention of MT-III could also affect cell survival, proliferation, differentiation, and gene expression by exchanging zinc with transcription factors or other nuclear metalloenzymes (12). It is intriguing to speculate that the hippocampal decrease we observed in MT-III in association with marked MFS and accumulation of neuronal zinc may contribute to reported patterns of neuronal losses in NBD.

Although a role for MT in protection from the toxic effects of heavy metals and other xenobiotics has been described, the potentially deleterious effects of MT induction during brain development have not been addressed. In the aged rat hippocampus, MT-I, -II, and -III levels increase compared to young rats, with a concomitant decrease in free zinc ion bioavailability and hippocampal zinc content. High levels of MT under stress conditions may adversely affect zinc-dependent antioxidant enzyme activity, DNA repair, and/or synaptic transmission by reducing free zinc ion bioavailability (39). The astrocytic MT-I/-II and MT-III responses in the CNS of NBD rats may also interfere with normal brain development by sequestering zinc from specific neuronal populations. Induction of MT in NBD or other CNS viral infections may result in harmful sequestration of toxic heavy metals. Even low dose exposure to trace metals such as nickel or mercury may aggravate disease associated with coxsackievirus B type 3 and herpes simplex virus type 2 infection (18, 26). Thus, the MT response may be saturated in the maturing host, reducing the capacity to respond to the burden of additional stressors in the wake of persistent viral infection.

Zinc is important in normal neurotransmission and neuromodulation but contributes to neuronal death in seizure, ischemia, hypoglycemia, and mechanical trauma models of brain injury (13, 20, 33, 55, 56, 60). Although the mechanism of zinc-induced cell death has not been clearly established, zinc can inhibit key glycolytic enzymes, trigger caspase activation and apoptosis via the $p75^{NTR}$ pathway, and activate poly(ADP-ribose) polymerase (PARP) which depletes cellular NAD^+ (30, 44, 51).

In NBD, zinc is decreased in mossy fiber boutons and accumulates in glial cells and somata of degenerating dentate gyrus granule cells. Indeed, zinc is only present in those granule cell neurons with morphological signs of neurodegeneration. In NBD rats we detected a specific increase in PARP expression in zinc-positive dentate gyrus granule cells, suggesting that zinc-mediated activation of PARP may play a role in granule cell death. Although we cannot unequivocally demonstrate zinc toxicity pharmacologically because this would require chronic chelation, confounding developmental pathways where zinc is critical, our data are consistent with a role for zinc in the selective neuronal losses by apoptosis that have been demonstrated in NBD rats.

ZnT-3 is localized to membranes of synaptic vesicles in a subset of glutamatergic neurons that correspond to pathways in which zinc is detected by the Timm reaction (43, 63). In NBD, ZnT-3 mRNA is reduced in hippocampus, and ZnT-3 protein and zinc (Timm stain signal) are decreased in granule cell mossy fibers. The observation of decreased zinc in mossy fiber pathways in NBD is consistent with decreased ZnT-3 and the defined role for ZnT-3 in controlling vesicular zinc (15). Reduced Timm staining in mossy fibers may also result from pathological release of excess Zn^{2+} into the extracellular space by zinc-enriched boutons. In NBD, increased levels of MT-I/-II and MT-III in hippocampal astrocytes and of ZnT-3 in glial cells may represent a compensatory mechanism to enhance sequestration of free zinc in the context of reduced neuronal ZnT-3 mRNA and protein. However, the decrease in ZnT-3 immunostaining and zinc signal in mossy fibers is likely attributable to the loss of granule cell neurons in NBD.

Mossy fiber sprouting is one of the most extensively investigated manifestations of synaptic plasticity and is described in temporal lobe epilepsy and epilepsy induced by kainic acid, pilocarpine, or electroconvulsive shock; lesioning of the hippocampus; trauma; stroke; and infection with feline immunodeficiency or herpes viruses (11, 50). The synaptic reorganization and expression of neuroplasticity markers (ie, synaptophysin and GAP-43) observed in some hippocampal seizure models is reminiscent of findings in NBD rats (4, 22, 35). Here, we report that 2 additional molecules implicated in synaptic plasticity and MFS, TN-R and CD44, are increased in NBD (4, 5, 10, 64). TN-R is implicated in the evolution and perpetuation of persistent CNS disease associated with increased excitatory transmission such as epilepsy (46). The hyaluronan receptor, CD44, assists axonal pathfinding during development and is increased in the brain following ischemia, nerve transection, and brain trauma (28, 36, 61). Neonatal rodent models of experimentally-induced seizures are associated with cognitive deficits in visual-spatial learning and memory that are paralleled by MFS (53). In NBD, progressive damage to dentate gyrus coincides with deficits in spatial learning and memory (45). Zinc dysregulation and associated MFS in NBD

may lead to cognitive and behavioral deficits by disrupting neural plasticity mechanisms in hippocampal zinc-enriched neurons.

There is increasing evidence that zinc contributes to CNS dysfunction and degeneration in epilepsy, transient global ischemia, brain trauma, Alzheimer disease, amyotrophic lateral sclerosis (ALS), Parkinson disease, and HIV neuropathology/AIDS dementia complex (ADC) (17). Our findings of alterations in zinc distribution, ZnT-3 expression, and astrocytic MT-I/-II and MT-III induction, in combination with previously described cytokine and apoptosis product alterations in NBD rats, suggests a multifactorial pathway leading to selective damage. The accumulation of zinc in degenerating granule cells in NBD and the subsequent losses of dentate gyrus granule cells is consistent with selective neuronal death in models of epilepsy, ischemia, hypoglycemia, and brain trauma. NBD provides a unique viral model for studying regulatory mechanisms for zinc homeostasis, endogenous/exogenous heavy metal toxicity, and metallothioneins in the context of neural development.

ACKNOWLEDGMENTS

This work was supported by National Institutes of Health Award NS29425 (WIL), HD37546 (WIL), and MH01608 (MH). We are grateful to Dr. Richard Palmiter for his gift of antibodies to ZnT-3 and Dr. Juan Hidalgo for his gift of antibodies to MT-III.

REFERENCES

1. Anderson CM, Swanson RA (2000) Astrocyte glutamate transport: review of properties, regulation, and physiological functions. *Glia* 32:1-14.

2. Aschner M, Cherian MG, Klaassen CD, Palmiter RD, Erickson JC, Bush AI (1997) Metallothioneins in brain-the role in physiology and pathology. *Toxicol Appl Pharmacol* 142:229-242.

3. Billaud JN, Ly C, Phillips TR, de la Torre JC (2000) Borna disease virus persistence causes inhibition of glutamate uptake by feline primary cortical astrocytes. *J Virol* 74:10438-10446.

4. Borges K, McDermott DL, Dingledine R (2004) Reciprocal changes of CD44 and GAP-43 expression in the dentate gyrus inner molecular layer after status epilepticus in mice. *Exp Neurol* 188:1-10.

5. Brenneke F, Schachner M, Elger CE, Lie AA (2004) Up-regulation of the extracellular matrix glycoprotein tenascin-R during axonal reorganization and astrogliosis in the adult rat hippocampus. *Epilepsy Res* 58:133-143.

6. Carbone KM, Rubin SA, Nishino Y, Pletnikov MV (2001) Borna disease: virus-induced neurobehavioral disease pathogenesis. *Curr Opin Microbiol* 4:467-475.

7. Carrasco J, Giralt M, Molinero A, Penkowa M, Moos T, Hidalgo J (1999) Metallothionein (MT)-III: generation of polyclonal antibodies, comparison with MT-I+II in the freeze lesioned rat brain and in a bioassay with astrocytes, and analysis of Alzheimer's disease brains. *J Neurotrauma* 16:1115-1129.

8. Carrasco J, Penkowa M, Giralt M, Camats J, Molinero A, Campbell IL, Palmiter RD, Hidalgo J (2003) Role of metallothionein-III following central nervous system damage. *Neurobiol Dis* 13:22-36.

9. Cavazos JE, Golarai G, Sutula TP (1991) Mossy fiber synaptic reorganization induced by kindling: time course of development, progression, and permanence. *J Neurosci* 11:2795-2803.

10. Celio MR, Blumcke I (1994) Perineuronal nets--a specialized form of extracellular matrix in the adult nervous system. *Brain Res Rev* 19:128-145.

11. Chen SF, Huang CC, Wu HM, Chen SH, Liang YC, Hsu KS (2004) Seizure, neuron loss, and mossy fiber sprouting in herpes simplex virus type 1-infected organotypic hippocampal cultures. *Epilepsia* 45:322-332.

12. Cherian MG, Apostolova MD (2000) Nuclear localization of metallothionein during cell proliferation and differentiation. *Cell Mol Biol* 46:347-356.

13. Choi DW, Koh JY (1998) Zinc and brain injury. *Annu Rev Neurosci* 21:347-375.

14. Chung RS, Vickers JC, Chuah MI, Eckhardt BL, West AK (2002) Metallothionein-III inhibits initial neurite formation in developing neurons as well as postinjury, regenerative neurite sprouting. *Exp Neurol* 178:1-12.

15. Cole TB, Wenzel HJ, Kafer KE, Schwartzkroin PA, Palmiter RD (1999) Elimination of zinc from synaptic vesicles in the intact mouse brain by disruption of the ZnT3 gene. *Proc Natl Acad Sci U S A* 96:1716-1721.

16. Coyle P, Philcox JC, Carey LC, Rofe AM (2002) Metallothionein: the multipurpose protein. *Cell Mol Life Sci* 59:627-647.

17. Cuajungco MP, Lees GJ (1997) Zinc metabolism in the brain: relevance to human neurodegenerative disorders. *Neurobiol Dis* 4:137-169.

18. Ellermann-Eriksen S, Christensen MM, Mogensen SC (1994) Effect of mercuric chloride on macrophage-mediated resistance mechanisms against infection with herpes simplex virus type 2. *Toxicology* 93:269-287.

19. Frederickson CJ (1989) Neurobiology of zinc and zinc-containing neurons. *Int Rev Neurobiol* 31:145-238.

20. Frederickson CJ, Hernandez MD, McGinty JF (1989) Translocation of zinc may contribute to seizure-induced death of neurons. *Brain Res* 480:317-321.

21. Ghoshal K, Majumder S, Zhu Q, Hunzeker J, Datta J, Shah M, Sheridan JF, Jacob ST (2001) Influenza virus infection induces metallothionein gene expression in the mouse liver and lung by overlapping but distinct molecular mechanisms. *Mol Cell Biol* 21:8301-8317.

22. Gonzalez-Dunia D, Watanabe M, Syan S, Mallory M, Masliah E, De La Torre JC (2000) Synaptic pathology in Borna disease virus persistent infection. *J Virol* 74:3441-3448.

23. Heuchel R, Radtke F, Georgiev O, Stark G, Aguet M, Schaffner W (1994) The transcription factor MTF-1 is essential for basal and heavy metal-induced metallothionein gene expression. *Embo J* 13:2870-2875.

24. Hidalgo J, Aschner M, Zatta P, Vasak M (2001) Roles of the metallothionein family of proteins in the central nervous system. *Brain Res Bull* 55:133-145.

25. Hornig M, Weissenbock H, Horscroft N, Lipkin WI (1999) An infection-based model of neurodevelopmental damage. *Proc Natl Acad Sci U S A* 96:12102-12107.

26. Ilback NG, Fohlman J, Friman G (1994) Changed distribution and immune effects of nickel augment viral-induced inflammatory heart lesions in mice. *Toxicology* 91:203-219.

27. Ilback NG, Glynn AW, Wikberg L, Netzel E, Lindh U (2004) Metallothionein is induced and trace element balance changed in target organs of a common viral infection. *Toxicology* 199:241-250.

28. Jones LL, Liu Z, Shen J, Werner A, Kreutzberg GW, Raivich G (2000) Regulation of the cell adhesion molecule CD44 after nerve transection and direct trauma to the mouse brain. *J Comp Neurol* 426:468-492.

29. Kelly EJ, Quaife CJ, Froelick GJ, Palmiter RD (1996) Metallothionein I and II protect against zinc deficiency and zinc toxicity in mice. *J Nutr* 126:1782-1790.

30. Kim YH, Koh JY (2002) The role of NADPH oxidase and neuronal nitric oxide synthase in zinc-induced poly(ADP-ribose) polymerase activation and cell death in cortical culture. *Exp Neurol* 177:407-418.

31. Klaassen CD, Liu J (1998a) Metallothionein transgenic and knock-out mouse models in the study of cadmium toxicity. *J Toxicol Sci* 23 Suppl 2:97-102.

32. Klaassen CD, Liu J (1998b) Induction of metallothionein as an adaptive mechanism affecting the magnitude and progression of toxicological injury. *Environ Health Perspect* 106 Suppl 1:297-300.

33. Koh JY, Suh SW, Gwag BJ, He YY, Hsu CY, Choi DW (1996) The role of zinc in selective neuronal death after transient global cerebral ischemia. *Science* 272:1013-1016.

34. Lee JY, Kim JH, Palmiter RD, Koh JY (2003) Zinc released from metallothionein-iii may contribute to hippocampal CA1 and thalamic neuronal death following acute brain injury. *Exp Neurol* 184:337-347.

35. Li S, Reinprecht I, Fahnestock M, Racine RJ (2002) Activity-dependent changes in synaptophysin immunoreactivity in hippocampus,

piriform cortex, and entorhinal cortex of the rat. *Neuroscience* 115:1221-1229.

36. Lin L, Chan SO (2003) Perturbation of CD44 function affects chiasmatic routing of retinal axons in brain slice preparations of the mouse retinofugal pathway. *Eur J Neurosci* 17:2299-2312.

37. Liu J, Ying W, Massa S, Duriez PJ, Swanson RA, Poirier GG, Sharp FR (2000) Effects of transient global ischemia and kainite on poly(ADP-ribose) polymerase (PARP) gene expression and proteolytic cleavage in gerbil and rat brains. *Mol Brain Res* 80:7-16.

38. Masters BA, Quaife CJ, Erickson JC, Kelly EJ, Froelick GJ, Zambrowicz BP, Brinster RL, Palmiter RD (1994) Metallothionein III is expressed in neurons that sequester zinc in synaptic vesicles. *J Neurosci* 14:5844-5857.

39. Mocchegiani E, Giacconi R, Fattoretti P, Casoli T, Cipriano C, Muti E, Malavolta M, DiStefano G, Bertoni-Freddari C (2004) Metallothionein isoforms (I+II and III) and interleukin-6 in the hippocampus of old rats: may their concomitant increments lead to neurodegeneration? *Brain Res Bull* 63:133-142.

40. Moos T (1993) Simultaneous application of Timm sulphide silver method and immunofluorescence histochemistry. *J Neurosci Methods* 48:149-156.

41. Mucke L, Eddleston M (1993) Astrocytes in infectious and immune-mediated diseases of the central nervous system. *FASEB J* 7:1226-1232.

42. Narayan O, Herzog S, Frese K, Scheefers H, Rott R (1983) Behavioral disease in rats caused by immunopathological responses to persistent Borna virus in the brain. *Science* 220:1401-1403.

43. Palmiter RD, Cole TB, Quaife CJ, Findley SD (1996) ZnT-3, a putative transporter of zinc into synaptic vesicles. *Proc Natl Acad Sci U S A* 93:14934-14939.

44. Park JA, Lee JY, Sato TA, Koh JY (2000) Co-induction of p75NTR and p75NTR-associated death executor in neurons after zinc exposure in cortical culture or transient ischemia in the rat. *J Neurosci* 20:9096-9103.

45. Rubin SA, Sylves P, Vogel M, Pletnikov M, Moran TH, Schwartz GJ, Carbone KM (1999) Borna disease virus-induced hippocampal dentate gyrus damage is associated with spatial learning and memory deficits. *Brain Res Bull* 48:23-30.

46. Saghatelyan AK, Dityatev A, Schmidt S, Schuster T, Bartsch U, Schachner M (2001) Reduced perisomatic inhibition, increased excitatory transmission, and impaired long-term potentiation in mice deficient for the extracellular matrix glycoprotein tenascin-R. *Mol Cell Neurosci* 17:226-240.

47. Sato M, Sasaki M, Hojo H (1994) Differential induction of metallothionein synthesis by interleukin-6 and tumor necrosis factor-alpha in rat tissues. *Int J Immunopharmacol* 16:187-195.

48. Sauder C, de la Torre JC (1999) Cytokine expression in the rat central nervous system following perinatal Borna disease virus infection. *J Neuroimmunol* 96:29-45.

49. Sawashita J, Takeda A, Okada S (1997) Change of zinc distribution in rat brain with increasing age. *Dev Brain Res* 102:295-298.

50. Scharfman HE, Sollas AL, Berger RE, Goodman JH (2003) Electrophysiological evidence of monosynaptic excitatory transmission between granule cells after seizure-induced mossy fiber sprouting. *J Neurophysiol* 90:2536-2547.

51. Sheline CT, Behrens MM, Choi DW (2000) Zinc-induced cortical neuronal death: contribution of energy failure attributable to loss of NAD(+) and inhibition of glycolysis. *J Neurosci* 20:3139-3146.

52. Sloviter RS (1982) A simplified Timm stain procedure compatible with formaldehyde fixation and routine paraffin embedding of rat brain. *Brain Res Bull* 8:771-774.

53. Sogawa Y, Monokoshi M, Silveira DC, Cha BH, Cilio MR, McCabe BK, Liu X, Hu Y, Holmes GL (2001) Timing of cognitive deficits following neonatal seizures: relationship to histological changes in the hippocampus. *Dev Brain Res* 131:73-83.

54. Song H, Stevens CF, Gage FH (2002) Astroglia induce neurogenesis from adult neural stem cells. *Nature* 417:39-44.

55. Suh SW, Garnier P, Aoyama K, Chen Y, Swanson RA (2004) Zinc release contributes to hypoglycemia-induced neuronal death. *Neurobiol Dis* 16:538-545.

56. Suh SW, Chen JW, Motamedi M, Bell B, Listiak K, Pons NF, Danscher G, Frederickson CJ (2000) Evidence that synaptically-released zinc contributes to neuronal injury after traumatic brain injury. *Brain Res* 852:268-273.

57. Takeda A (2000) Movement of zinc and its functional significance in the brain. *Brain Res Rev* 34:137-148.

58. Uchida Y, Takio K, Titani K, Ihara Y, Tomonaga M (1991) The growth inhibitory factor that is deficient in the Alzheimer's disease brain is a 68 amino acid metallothionein-like protein. *Neuron* 7:337-347.

59. Vallee BL, Falchuk KH (1993) The biochemical basis of zinc physiology. *Physiol Rev* 73:79-118.

60. Vandenberg RJ, Mitrovic AD, Johnston GA (1998) Molecular basis for differential inhibition of glutamate transporter subtypes by zinc ions. Mol Pharmacol 54:189-196.

61. Wang H, Zhan Y, Xu L, Feuerstein GZ, Wang X (2001) Use of suppression subtractive hybridization for differential gene expression in stroke: discovery of CD44 gene expression and localization in permanent focal stroke in rats. *Stroke* 32:1020-1027.

62. Weissenbock H, Hornig M, Hickey WF, Lipkin WI (2000) Microglial activation and neuronal apoptosis in Bornavirus infected neonatal Lewis rats. *Brain Pathol* 10:260-272.

63. Wenzel HJ, Cole TB, Born DE, Schwartzkroin PA, Palmiter RD (1997) Ultrastructural localization of zinc transporter-3 (ZnT-3) to synaptic vesicle membranes within mossy fiber boutons in the hippocampus of mouse and monkey. *Proc Natl Acad Sci U S A* 94:12676-12681.

64. Wintergerst ES, Fuss B, Bartsch U (1993) Localization of janusin mRNA in the central nervous system of the developing and adult mouse. *Eur J Neurosci* 5:299-310.

65. Yagle MK, Palmiter RD (1985) Coordinate regulation of mouse metallothionein I and II genes by heavy metals and glucocorticoids. *Mol Cell Biol* 5:291-294.

66. Yokoyama M, Koh J, Choi DW (1986) Brief exposure to zinc is toxic to cortical neurons. *Neurosci Lett* 71:351-355.

67. You HJ, Oh DH, Choi CY, Lee DG, Hahm KS, Moon AR, Jeong HG (2002) Protective effect of metallothionein-III on DNA damage in response to reactive oxygen species. *Biochim Biophys Acta* 1573:33-38.